J. Membrane Biol. 174, 71–83 (2000)

The Journal of
Membrane
Biology

Cation Permeability and Selectivity of a Root Plasma Membrane Calcium Channel

P.J. White[1], M. Piñeros[2,*], M. Tester[3], M.S. Ridout[4]

[1]Department of Plant Genetics and Biotechnology, Horticulture Research International, Wellesbourne, Warwick CV35 9EF, UK
[2]Department of Botany, University of Adelaide, Adelaide, SA, Australia
[3]Department of Plant Sciences, University of Cambridge, Downing Street, Cambridge CB2 3EA, UK
[4]Department of Biometrics, Horticulture Research International, East Malling, West Malling, Kent ME19 6BJ, UK

Received: 23 August 1999/Revised: 12 November 1999

Abstract. Calcium channels in the plasma membrane of root cells fulfill both nutritional and signaling roles. The permeability of these channels to different cations determines the magnitude of their cation conductances, their effects on cell membrane potential and their contribution to cation toxicities. The selectivity of the *rca* channel, a Ca^{2+}-permeable channel from the plasma membrane of wheat (*Triticum aestivum* L.) roots, was studied following its incorporation into planar lipid bilayers. The permeation of K^+, Na^+, Ca^{2+} and Mg^{2+} through the pore of the *rca* channel was modeled. It was assumed that cations permeated in single file through a pore with three energy barriers and two ion-binding sites. Differences in permeation between divalent and monovalent cations were attributed largely to the affinity of the ion binding sites. The model suggested that significant negative surface charge was present in the vestibules to the pore and that the pore could accommodate two cations simultaneously, which repelled each other strongly. The pore structure of the *rca* channel appeared to differ from that of L-type calcium channels from animal cell membranes since its ion binding sites had a lower affinity for divalent cations. The model adequately accounted for the diverse permeation phenomena observed for the *rca* channel. It described the apparent submillimolar K_m for the relationship between unitary conductance and Ca^{2+} activity, the differences in selectivity sequences obtained from measurements of conductance and permeability ratios, the changes in relative cation permeabilities with solution ionic composition, and the complex effects of Ca^{2+} on K^+ and Na^+ currents through the channel. Having established the adequacy of the model, it was used to predict the unitary currents that would be observed under the ionic conditions employed in patch-clamp experiments and to demonstrate the high selectivity of the *rca* channel for Ca^{2+} influx under physiological conditions.

Key words: Calcium (Ca^{2+}) — Permeation — Planar lipid bilayer — Potassium (K^+) — *rca* channel — Wheat (*Triticum aestivum* L.)

Introduction

Calcium-permeable channels in the plasma membrane of root cells have been studied electrically following their reconstitution into planar lipid bilayers (PLB; Piñeros & Tester, 1997; White, 1997, 1998) and by patch-clamping protoplasts from root cells (Thion et al., 1998; Kiegle, Haseloff & Tester, 1998). When plasma-membrane vesicles from wheat roots are incorporated into PLB a calcium-permeable channel, termed the *rca* channel, is frequently observed (Piñeros & Tester, 1995, 1997*a*). The *rca* channel is permeable to a wide variety of monovalent and divalent cations and opens upon plasma membrane depolarization (Piñeros & Tester, 1995, 1997*a*). The *rca* channel is inhibited by a range of pharmaceuticals including Al^{3+}, La^{3+}, Gd^{3+}, verapamil, diltiazem and ruthenium red, but it is insensitive to 1,4-dihydropyridines and bepridil (Piñeros & Tester, 1995, 1997*a*,*b*). A channel with similar biophysical characteristics was observed when plasma-membrane vesicles from rye roots were incorporated into PLB (White, 1994, 1998). It has been argued that the physiological role of the *rca* channel is to mediate Ca^{2+} influx upon plasma membrane depolarization and, thereby, to increase the cyto-

* *Present address:* U.S. Plant, Soil and Nutrition Laboratory, Cornell University, Tower Road, Ithaca, NY 14853-00001, USA

Correspondence to: P.J. White

plasmic Ca^{2+} concentration ($[Ca^{2+}]_{cyt}$). Depolarization can be elicited by many environmental, developmental or pathological challenges and an increase in $[Ca^{2+}]_{cyt}$ is thought to initiate a physiological response.

Measurements of single-channel conductance and ionic selectivity provide information on the biophysical mechanisms underlying ion permeation. In previous studies, the unitary-current *vs.* voltage (*I/V*) relationships obtained for the *rca* channel were fitted to the Goldman-Hodgkin-Katz (GHK) current equation (Piñeros & Tester, 1995, 1997*a*). However, a different ratio for cation permeabilities (P_K/P_{Ca}) was required to fit each set of ionic conditions and it is a precept of the GHK theory that a unique value of P_K/P_{Ca} exists. Thus, the GHK equation is inappropriate to describe cation permeation through the *rca* channel.

Several alternative models are available to describe the permeation of ions through the pore of a channel (Nonner & Eisenberg, 1998; Levitt, 1999; McCleskey, 1999; Miller, 1999; White et al., 1999). The model which has been most frequently applied to L-type Ca^{2+} channels in animal cell membranes is based on a "multi-ion" pore which contains two high affinity binding sites for cations separated by an insignificant energy barrier (e.g., Almers & McCleskey, 1984; Hess & Tsien, 1984; Hille, 1992; Yellen, 1993; Aidley & Stanfield, 1996; McCleskey, 1999). These sites have a high affinity for Ca^{2+}, the dissociation constant (K_d) being in the micromolar range. Monovalent cations, which have a lower affinity for these sites, can permeate in the absence of Ca^{2+}. However, when Ca^{2+} is present it preferentially occupies the binding sites thereby reducing both the flux of monovalent cations and the unitary current. When both sites are occupied by Ca^{2+}, there is a strong electrostatic repulsion, elevating the free-energy of Ca^{2+} at the binding sites. This increase in the free-energy of Ca^{2+} at the binding sites accelerates Ca^{2+} movement and accounts for the differences between the apparent K_i for the reduction of monovalent cation flux and unitary current (micromolar: single occupancy) and the apparent K_m for divalent cation permeation (millimolar: double occupancy). This classic model has also been used to describe cation permeation through the Ca^{2+}-permeable high-conductance "maxi" cation channel in the plasma membrane of plant roots (White & Ridout, 1999).

In this paper a similar model is used to describe cation permeation through the *rca* channel. The pore of the *rca* channel is modeled as a "multi-ion" pore that has three energy-barriers and two ion-binding sites (a 3B2S model). It is assumed that cations permeate in single file. More than one cation can be present, and cations can interact, within the pore. The use of this model was suggested by the observations: (i) that the selectivity sequences obtained from measurements of conductance and permeability ratios differed (Piñeros, 1995), (ii) that apparent permeability ratios changed with cation concentration (Piñeros & Tester, 1995, 1997*a*; White, 1997), and (iii) that an anomalous mole fraction effect (minimum) is observed in the inward unitary conductance as the ratio of $BaCl_2$ to $CaCl_2$ (at a total concentration of 1 mM divalent cation) is varied in the extracellular medium and 1 mM $CaCl_2$ is present in the cytoplasmic medium (Piñeros, 1995). All these are characteristics of L-type Ca^{2+} channels in animal cell membranes and of "multi-ion" pores in general (Hille, 1992).

The structural characteristics of the pore and the free-energy profiles for K^+, Na^+, Ca^{2+} and Mg^{2+} were estimated. This allowed the permeation pathway of the *rca* channel to be compared with that of other Ca^{2+}-permeable channels in plant and animal cell membranes. The permeation model was used to predict the unitary currents that would be observed in patch-clamp experiments on the *rca* channel and to demonstrate the high selectivity of the *rca* channel for Ca^{2+} influx under physiological ionic conditions. It is argued that, if coupled to an appropriate kinetic model, the permeation model could also be used to predict ionic fluxes through the *rca* channel under changing physiological conditions.

Materials and Methods

Plasma Membrane Isolation and Incorporation into Planar Lipid Bilayers

Wheat (*Triticum aestivum* L.) caryopses were imbibed in distilled water for 36 to 48 hr and, following germination, grown in darkness over a 1 mM $CaSO_4$ solution. Roots were harvested on the fourth day after germination and plasma-membrane vesicles were obtained by aqueous-polymer two-phase partitioning of a microsomal-membrane fraction (Piñeros & Tester, 1995).

Plasma-membrane vesicles were incorporated into PLB generated from a dispersion of 8 mM PE, 3 mM PS, 1.5 mM PC and 12.5 mM cholesterol in *n*-decane, as described by Piñeros & Tester (1995). The bilayer separated volumes of 500 μl in the *cis* compartment and 1.5 ml in the *trans* compartment. Plasma-membrane vesicles were added to the solution in the *cis* compartment and, following incorporation, the *rca* channel became orientated with its extracellular surface facing the *cis* solution (Piñeros & Tester, 1995).

The orientation, conductivity and voltage dependence of the *rca* channel were determined prior to experimentation. Since verapamil reduced the current through the *rca* channel only when applied to the extracellular face of the channel (Piñeros & Tester, 1995), channel orientation was verified by the addition of 1–10 μM verapamil to the solution in the *cis* chamber. The *cis* chamber was then perfused with 1 mM $CaCl_2$ and the unitary conductance and voltage-dependence of the channel were estimated to confirm its identity.

Ionic conditions were established either by the addition of stock solutions or by perfusing the *cis* chamber with an appropriate solution. Unless indicated, $CaCl_2$ and other cation chloride solutions were unbuffered and their pH was adjusted to 5.5 by addition of HCl. Potassium was supplied as KCl, and solutions containing KCl also contained 0.8 mM $CaCl_2$, 0.8 mM ethylene glycol-bis (β-aminoethyl-ether) N,N,-N′,N′-tetraacetic acid (EGTA), pH 7.0 (adjusted with KOH). The Ca^{2+}

activity under these conditions was 500 nM. Ionic activities and speciation were calculated using GEOCHEM-PC version 2.0 (Parker, Norvell & Chaney, 1995).

Single Channel Recordings

Experiments were performed at room temperature. Current recordings were obtained under voltage-clamp conditions using a Dagan 3900A amplifier (with 3910 expander; Dagan, Minneapolis, MN) connected to the bilayer chambers via 3 M KCl/1% agar salt bridges. Voltages were referenced to the *cis* chamber, which was grounded. This accords with the physiological convention (i.e., cytosol with respect to the external medium). Movement of cations from the extracellular to the cytoplasmic side of the channel is indicated by a negative current. Data were stored unfiltered on digital audiotape (DTC-75ES; Sony, Japan). To determine unitary currents, data were replayed, filtered at 100 Hz with an 8-pole low pass Bessel filter (Series 902, Frequency Devices, Haverhill, MA) and displayed on a digital storage oscilloscope (Gould 400, Gould Electronics, Hainault, UK).

Several of the data sets have been published previously (Piñeros & Tester, 1995, 1997*a*) and the remainder can be found in Piñeros (1995). Examples of single-channel current recordings can also be found in these papers. In addition to the data presented in the figures, *I/V* relationships obtained in solutions containing (*trans*:*cis*) 0.05:0.01, 0.05:0.02, 0.05:10, 0.05:1000, 0.1:0.005, 0.1:0.02, 0.1:0.05 mM $CaCl_2$ and 150 mM NaCl plus 1.5 mM free Ca^{2+}:50 μM $CaCl_2$ were also input for regressions. Since no attempt was made to standardize data from different experiments (with the exception that the data presented in Fig. 7 were scaled so that the unitary conductance determined between +100 and −100 mV in the presence of symmetrical 1 mM $CaCl_2$ was 20 pS), it should be noted that *rca* channel activities from different membrane preparations can differ in their unitary currents (e.g., legend to Fig. 8).

Modeling

Estimates of energy profiles for permeant cations and structural characteristics of the *rca* channel were obtained using a version of the FORTRAN computer program AJUSTE (Alvarez, Villarroel & Eisenman, 1992) modified for the presence of both monovalent and divalent cations (White & Ridout, 1999). The model chosen (a 3B2S model) had energy profiles consisting of three energy-barriers and two ion binding-sites (energy-wells), and allowed for single-file permeation, double cation occupancy, ion-ion repulsion and surface potential effects. The energies of the unoccupied channel at zero voltage (expressed as multiples of the thermal energy, RT) were defined by three peaks G1, G2 and G3, and two wells, U1 and U2, with the postscript referring to their position relative to the *trans* (cytoplasmic) compartment. The distances D1 to D5 refer to the position of successive peaks and wells in the electrical field relative to the *trans* (cytoplasmic) compartment.

The effects of ion-ion interactions (electrostatic and/or allosteric) were simulated by the addition of an energy factor to the peaks and wells adjacent to an occupied well. This was calculated as $A(z_1z_2)/d$, where A is the ionic-repulsion energy parameter, z_1 and z_2 are the valencies of the interacting cations and d is the electrical distance from the occupied well. Two parameters (R_{scis} and R_{strans}) were included in the model to describe surface charge effects. These parameters correspond to the radii of circles (expressed in Å) containing one electron charge in the *cis* and *trans* vestibules of the pore respectively.

Rate constants were formulated by the standard Eyring rate theory expression equal to the product of a pre-exponential term, kT/h (where k/h is Boltzmann's constant divided by Planck's constant), and an exponential function of the energy difference, $\exp(\Delta G/(RT))$. A similar expression was used for the bimolecular rate constants describing the entry of ions from the internal or external solutions. The reference energy state of our model corresponds to 1 M solution. To compare our energy values to models that use a 55.5 M reference state (e.g., White & Ridout, 1995, 1999), 4.02 *RT* units must be subtracted from our values.

Following the precedent of previous workers (e.g., Alvarez et al., 1992; Allen, Sanders & Gradmann, 1998), parameters were estimated by weighted least squares with the weight taken as 1/current, subject to a maximal weighting of 0.5. This put greater weight on small currents and gave visually better coincidences. Parameters describing the free-energy profiles for K^+, Na^+ and Ca^{2+} permeation were fitted to the complete data set of 985 datapoints obtained in 39 different solution combinations in which these cations were present. Fitting began with a symmetrical model, with electrical distances of 0.00, 0.25, 0.50, 0.75 and 1.00 for D1 through D5, respectively. Starting parameters for well-depths were based on cation concentrations giving half-maximal conductance and for barrier heights on maximal cation conductances. Initially, models with fewer parameters were fitted to subsets of the data obtained in the presence of single cation species. These were then combined sequentially. Two contrasting sets of parameter estimates were pursued and the one with the lowest RSS is presented here. In total over 120 regressions were run in the course of obtaining the final parameters describing the free-energy profiles for K^+, Na^+ and Ca^{2+} permeation. Parameters describing the energies of the unoccupied channel at zero voltage (G1, G2, G3, U1 and U2) for Mg^{2+} were estimated using these values (Fig. 7).

Results

Pore Structure of the *rca* Channel

Traditionally, cation fluxes through the pores of Ca^{2+} channels have been modeled as the movement of cations through a corrugated free-energy profile (Hille, 1992; McCleskey, 1999). It is proposed that cations bind to specific sites within the pore and that each site can bind only one cation at a time. Such ion-binding sites are represented by energy minima. Energy barriers, representing restrictions to cation movement, separate each binding-site within the pore and also the pore from the solutions outside. Under certain conditions several ion-binding-sites may be occupied and cations simultaneously present within the pore will repel each other.

The pore of the *rca* channel was modeled with three energy barriers and two ion-binding sites (a 3B2S model). Single-file permeation was assumed. Although at the molecular level cations cannot pass each other within the pore of the channel, macroscopic (net) fluxes of different cationic species can occur in opposite directions. The direction of the net flux of a particular cation is determined by its electrochemical gradient. The magnitude of these net fluxes is determined by the probability of movements between cation binding sites and the external solutions.

Free-energy profiles for K^+, Na^+ and Ca^{2+} permeation of the *rca* channel (Table) were estimated using the

Table. Estimated parameters for the permeation of K^+, Na^+ and Ca^{2+} through the pore of the *rca* channel in the plasma membrane of wheat roots

	K^+	Na^+	Ca^{2+}
G1	1.98 ± 3.83	5.51 ± 2.82	0.83 ± 3.45
G2	−1.35*	2.87 ± 3.47	2.59 ± 3.61
G3	4.77 ± 3.72	−0.43 ± 4.74	1.04 ± 3.69
U1	−5.17 ± 1.39	−5.30 ± 2.96	−11.93 ± 3.51
U2	−6.01 ± 3.75	−6.61 ± 2.55	−12.80 ± 3.67
A		2.88 ± 1.15	
D1		0.04 ± 0.10	
D2		0.06 ± 0.10	
D3		0.57 ± 0.11	
D4		0.88 ± 0.10	
D5		0.92 ± 0.10	
R_{scis}		24.5 ± 2.65	
R_{strans}		38.0 ± 2.52	

Permeation is modeled as single-file movement through a free-energy profile with three energy barriers and two ion-binding sites that can be occupied simultaneously.

Parameters were estimated from *I/V* data collected across a wide variety of ionic conditions. The total number of observations was 985 and the weighted residual sum of squares was 234. Standard errors of parameter estimates are indicated. A reliable estimate of the standard error of G2 for K^+ (marked with an asterisk) is not available, but the parameter is estimated with low precision. The parameters G1, U1, G2, U2 and G3 define the free energies at electrical distances of D1, D2, D3, D4 and D5, respectively. They are expressed in (dimensionless) multiples of RT. The solution reference state is 1 M. The postscript refers to the position relative to the *trans* (cytoplasmic) compartment. The parameter A defines the magnitude of ionic interactions, which raise the free-energy profile by $A(z_1z_2)/d$, where z_1 and z_2 are the valencies of the interacting cations and d is the electrical distance from an occupied well. The parameters R_{scis} and R_{strans} (expressed in Å) correspond to the radii of circles containing one electron charge in the *cis* and *trans* vestibules of the pore, respectively.

complete data set obtained across a wide range of voltages and ionic conditions (985 observations from 39 different ionic conditions, of which 824 datapoints are presented in Figs. 1 to 7). Although better fits to *I/V* relationships for individual experiments could be obtained using slightly different parameter values, the estimates given here offer a representative description of the pore structure of the channel.

The pore structure described by the model had a slight asymmetry. The outermost free energy peaks (G1, G3) and the cation binding sites (U1, U2) were placed near the extremes of the pore. The central free-energy peak (G2) was close to the center of the pore. The relative magnitudes of free-energy peaks differed between cations. The outermost free-energy peaks were low for all cations, suggesting that entry into the channel was not particularly energetically unfavorable. The relative heights of the free-energy peak closest to the cytoplasm (G1) followed the sequence $Na^+ > K^+ > Ca^{2+}$, those of the central free-energy peak (G2) followed the sequence $Na^+ = Ca^{2+} > K^+$ and those of the peak closest to the exterior (G3) followed the sequence $K^+ > Ca^{2+} = Na^+$. The magnitudes of U1 and U2 for the two monovalent cations, K^+ and Na^+, were similar and greater than those for Ca^{2+}. The dissociation binding constants (K_ds) of the binding sites for K^+ and Na^+ in an unoccupied pore were between 1.3 and 5.7 mM, whereas those for Ca^{2+} were 6.6 μM (U1) and 2.8 μM (U2). These values can be compared with the apparent affinity of the channel for K^+ (K_m = 6 mM) and Ca^{2+} (K_m = 99 μM) obtained by fitting the Michaelis-Menten equation to the relationship between unitary conductance (estimated in nonsymmetrical or biionic conditions) and cation activity (Piñeros & Tester, 1997*a*). It is possible for the *rca* channel to be occupied by two cations simultaneously, and the strong interactions between cations within the pore may dominate conductance properties under certain conditions. The repulsion between cations would increase the free-energy of the unoccupied binding site in an occupied pore by 3.5 to 14.1 RT, depending upon the valency of the interacting cations. The model also indicated appreciable negative surface charge in both the cytoplasmic (0.0005 e/Å^2) and extracellular (0.0002 e/Å^2) vestibules of the pore.

All parameters except the central energy peak (G2) for K^+ permeation could be estimated with reasonable precision. However, the standard errors reported here for the free-energy parameters are larger than those from previous studies (e.g., White & Ridout, 1995, 1999). These estimates are highly correlated and the standard errors of the differences between barrier heights are much smaller. This implies that the entire energy profile can be shifted to greater or lesser values, but that the shape of the profile is better defined. An inability to estimate precisely the height of central energy peaks was also experienced in describing cation permeation through both a voltage-insensitive K^+ channel (White & Ridout, 1995) and the maxi cation channel (White & Ridout, 1999) in the plasma membrane of rye roots using 3B2S models.

Calcium Permeation

Unitary currents through the *rca* channel could be resolved at low micromolar Ca^{2+} concentrations (Piñeros & Tester, 1997*a*). This enabled *I/V* relationships to be determined under symmetrical conditions with Ca^{2+} concentrations of between 50 μM and 10 mM on both sides of the channel (Fig. 1). The 3B2S model described adequately the *I/V* relationships obtained in the presence of Ca^{2+} concentrations of 100 μM and above (Fig. 1*B–E*). It also described the low apparent K_m for the relationship between unitary conductance and Ca^{2+} activity (Fig. 1*F;* Piñeros & Tester, 1997*a*). The model was not able to

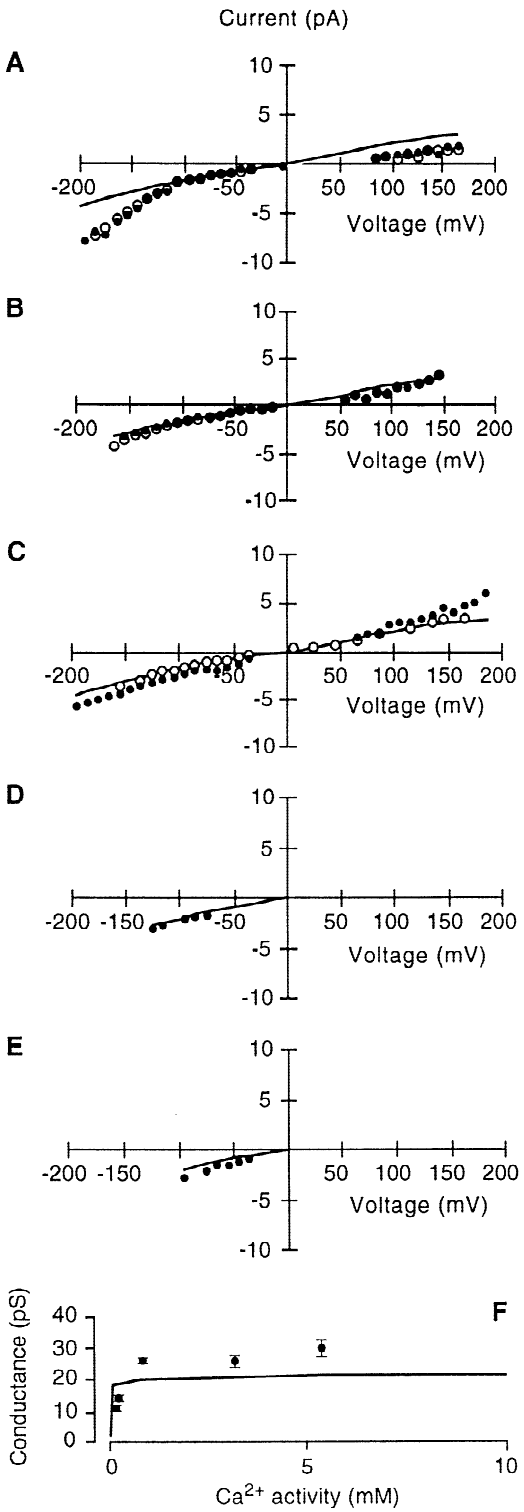

Fig. 1. (*A–E*) Unitary-current *vs.* voltage relationships and (*F*) unitary-conductance *vs.* Ca^{2+}-activity relationship for the *rca* channel from the plasma membrane of wheat roots assayed in the presence of symmetrical $CaCl_2$ solutions. Solutions contained (*A*) 50 μM (● $n = 5$ bilayers; ○ $n = 3$ bilayers), (*B*) 100 μM (● $n = 8$ bilayers; ○ $n = 3$ bilayers), (*C*) 1 mM (● $n = 11$ bilayers; ○ $n = 29$ bilayers), (*D*) 5 mM ($n = 3$ bilayers) and (*E*) 10 mM ($n = 4$ bilayers) $CaCl_2$. The different symbols indicate data from separate series of experiments. Unitary conductance was determined between ±100 mV and is expressed as mean ± SEM. Previously published data were taken from Piñeros & Tester (1995, 1997*a*). The curves are derived from a theoretical 3B2S model with the parameters shown in the Table.

describe either the decrease in unitary current at positive voltages nor the curious increase in unitary current at voltages more negative than about −100 mV when the Ca^{2+} concentration was reduced from 100 to 50 μM (Fig. 1*A*). One explanation for this phenomenon could be that the *rca* channel protein is directly affected by the ionic strength of the experimental solutions. This possibility is not considered in the proposed 3B2S model. However, it should also be noted that there was higher rectification and larger currents at high negative voltages at low Ca^{2+} concentrations in these experiments compared to others (*cf.* Fig. 2*A* and *B*). Such differences between experiments might reflect interactions between the *rca* channel and other components of the membrane preparation, such as lipids or accessory proteins, or a covalent modification of the *rca* channel protein itself (Bell, 1986; Hille, 1992; Aidley & Stanfield, 1996).

The *rca* channel has previously been shown to be highly selective for Ca^{2+} over Cl^- (Piñeros & Tester, 1995). In the present study, the selectivity of the *rca* channel was investigated over a wider range of ionic conditions, including low micromolar Ca^{2+} concentrations and steeper $CaCl_2$ gradients (Fig. 2). Currents always reversed near the theoretical (Nernst) reversal potential for Ca^{2+} and there was no indication of Cl^- permeability. The 3B2S model described the *I/V* relationships recorded in asymmetrical Ca^{2+} concentrations adequately (Fig. 2*A–L*). A difference between the fitted and observed *I/V* relationships was apparent under some ionic conditions (e.g., Fig. 2*E,G,I*), but no overall systematic deviation could be determined.

Interactions Between Calcium and Potassium During Permeation

The permeation of K^+, and the interaction of Ca^{2+} and K^+, within the pore of the *rca* channel was initially investigated under biionic conditions either by maintaining a high cytoplasmic (*trans*) K^+ concentration and varying extracellular Ca^{2+} activity (Fig. 3) or by maintaining a constant 100 μM extracellular Ca^{2+} activity and varying the cytoplasmic K^+ (Fig. 4). Under these conditions a small (26 to 36 pS) inward conductance and a large (59 to 220 pS) outward conductance was observed (Figs. 3 and 4).

Increasing the Ca^{2+} concentration on the extracellu-

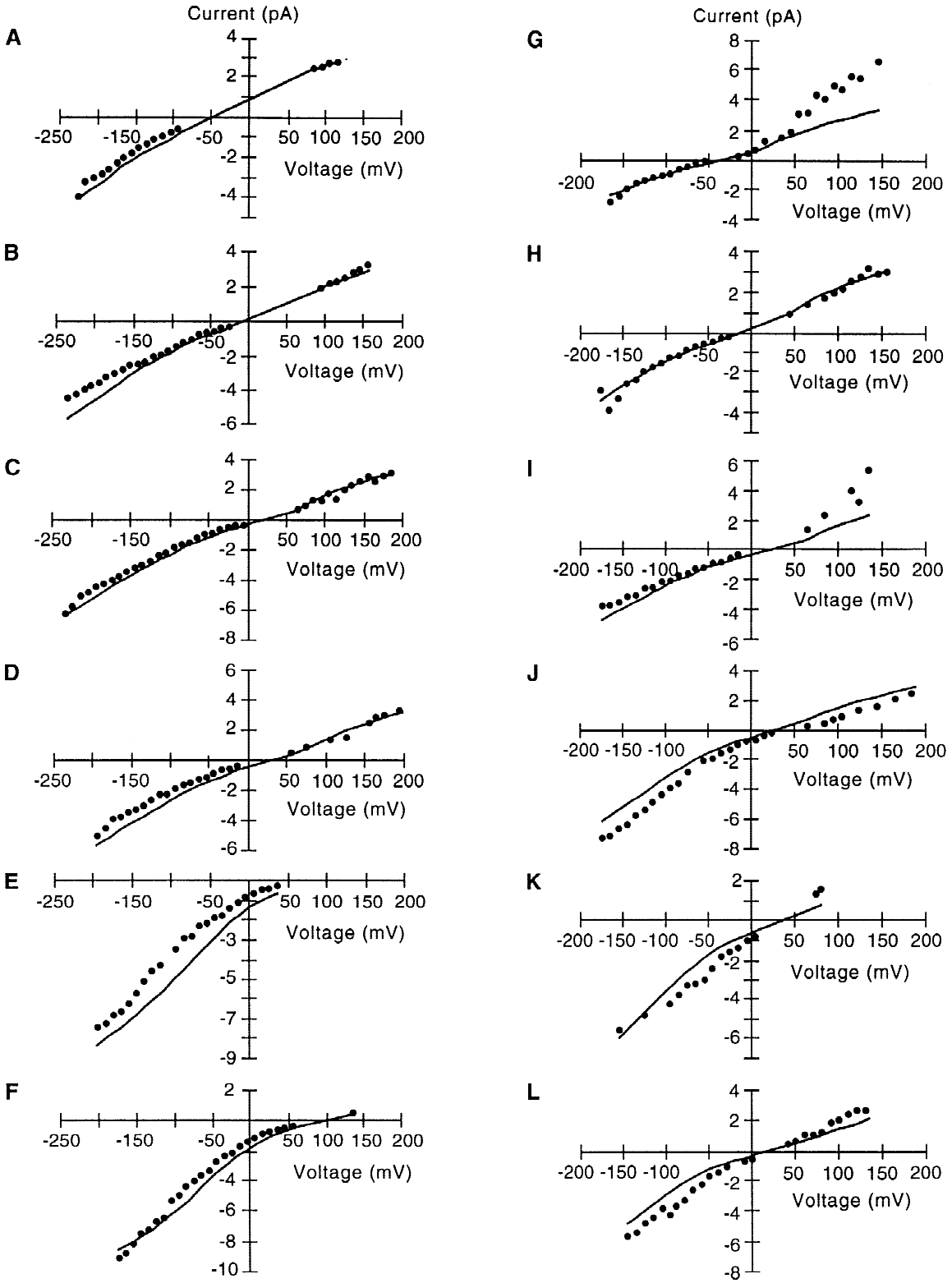

Fig. 2. Unitary-current *vs.* voltage relationships for the *rca* channel assayed in the presence of asymmetrical $CaCl_2$ solutions. Solutions contained *trans*:*cis* (*A*) 0.05:0.005 (n = 1 bilayer) (*B*) 0.05:0.1 (*C*) 0.05:0.50 (*D*) 0.05:1.0 (*E*) 0.05:50 (*F*) 0.05:500 (n = 1 bilayer) (*G*) 0.1:0.01 (n = 2 bilayers) (*H*) 0.1:0.07 (n = 4 bilayers) (*I*) 0.1:1.0 (*J*) 1:20 (*K*) 1:50 and (*L*) 10:95 mM $CaCl_2$. Data obtained in the presence of 1:20 mM and 10:95 mM $CaCl_2$ were taken from Piñeros & Tester (1995). Data are means from 3 bilayers unless indicated. The curves are derived from a theoretical 3B2S model with the parameters shown in the Table.

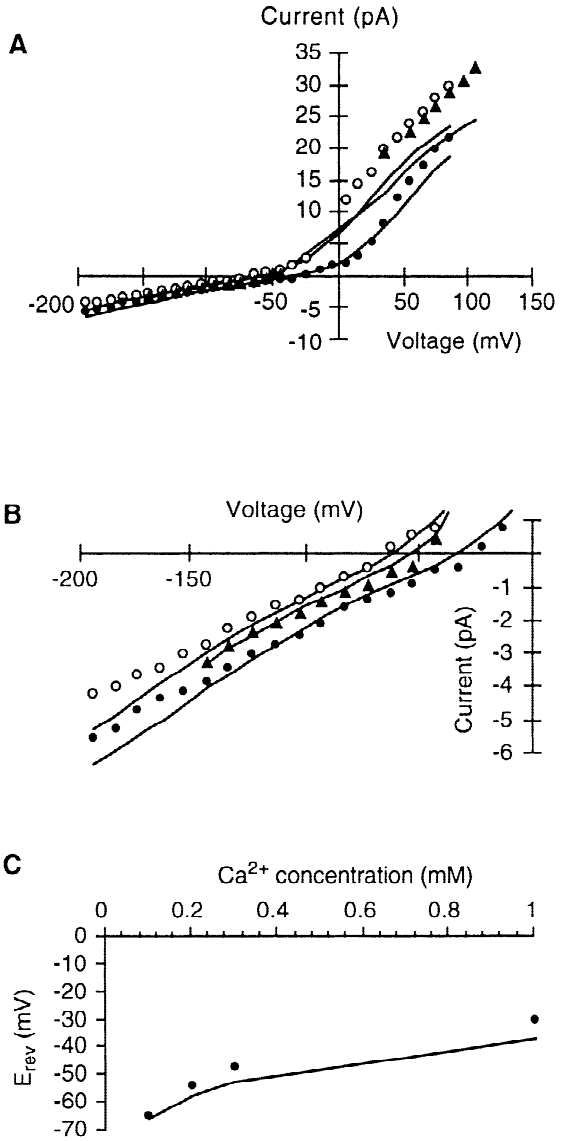

Fig. 3. (*A* and *B*) The effect of varying extracellular (*cis*) Ca^{2+} concentration on unitary-current *vs.* voltage relationships for the *rca* channel. (*C*) The relationship between the extracellular (*cis*) Ca^{2+} concentration and the current reversal potential (E_{rev}). The cytoplasmic face of the channel (*trans*) was exposed to 164 mM KCl (K^+ activity of 115 mM), 0.8 mM $CaCl_2$, 0.8 mM ethylene glycol-bis (β-aminoethyl-ether) N,N,N′,N′-tetraacetic acid (EGTA), pH 7.0 (adjusted with KOH). The Ca^{2+} activity, as estimated by GEOCHEM, was 500 mM. The extracellular face of the channel (*cis*) was exposed to 0.1 (○), 0.2 (▲) and 1 mM (●) $CaCl_2$, pH 5.5 (adjusted with HCl). Data were taken from Piñeros & Tester (1995). The curves are derived from a theoretical 3B2S model with the parameters shown in the Table.

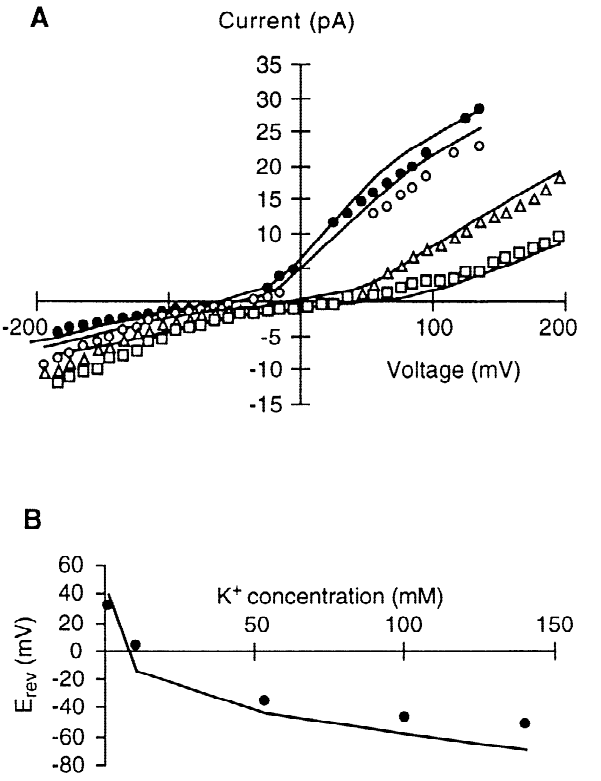

Fig. 4. (*A*) The effect of varying cytoplasmic (*trans*) K^+ concentration on unitary-current *vs.* voltage relationships for the *rca* channel from the plasma membrane of wheat roots. (*B*) The relationship between the cytoplasmic (*trans*) K^+ concentration and the current reversal potential (E_{rev}). The extracellular face of the channel (*cis*) was exposed to 100 μM $CaCl_2$, pH 5.5 (adjusted with HCl). The cytoplasmic face of the channel (*trans*) was exposed to concentrations of 140 (●), 100 (○), 10 (△) and 1 (□) mM KCl. All KCl solutions contained 0.8 mM $CaCl_2$, 0.8 mM EGTA, pH 7.0 (adjusted with KOH). The Ca^{2+} activity, as estimated by GEOCHEM, was 500 nM. Data were taken from Piñeros & Tester (1997*a*). The curves are derived from a theoretical 3B2S model with the parameters shown in the Table.

lar side from 0.1 to 1 mM in the presence of 164 mM K^+ plus 500 nM free Ca^{2+} on the cytoplasmic side resulted in a decrease in the magnitude of the outward current and a positive shift in E_{rev} (Fig. 3). Although the 3B2S model generally underestimated the unitary current observed at positive voltages, it did simulate the decline in unitary conductance at extreme positive voltages and the decrease in unitary current observed at positive voltages when the extracellular Ca^{2+} concentration was increased (Fig. 3*A*). The 3B2S model accurately fitted both the currents observed at negative voltages (Fig. 3*B*) and the positive displacement of E_{rev} as the extracellular Ca^{2+} concentration was increased (Fig. 3*C*). It can be noted that, since the apparent $P_{Ca}:P_K$ ratios calculated according to Fatt & Ginsborg (1958) from the observed E_{rev} values following the assumptions of GHK theory declined from 26 to 17 as the extracellular Ca^{2+} concentration was increased from 0.1 to 1 mM (Piñeros & Tester, 1995), it is inappropriate to describe permeation through the *rca* channel using GHK equations.

Increasing the K^+ concentration on the cytoplasmic side of the channel from 1 to 140 mM in the presence of 100 μM Ca^{2+} on the extracellular side increased the uni-

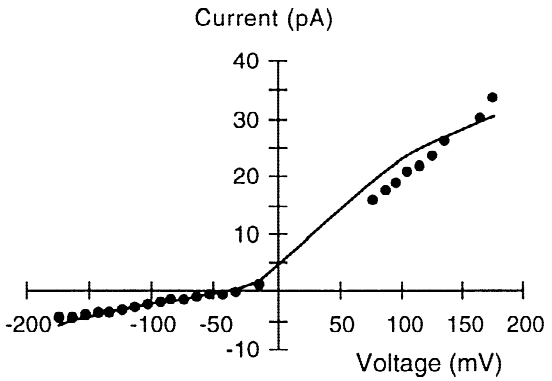

Fig. 5. Unitary-current *vs.* voltage relationships for the *rca* channel assayed under quasi physiological ionic conditions. The extracellular face of the channel (*cis*) was exposed to 1 mM KCl and 500 μM $CaCl_2$, pH 5.5 (adjusted with HCl). The cytoplasmic face of the channel (*trans*) was exposed to 140 mM KCl, 0.8 mM $CaCl_2$, 0.8 mM EGTA, pH 7.0 (adjusted with KOH). Free Ca^{2+} activity, as estimated by GEOCHEM, was 500 nM. Data were taken from Piñeros & Tester (1997*a*). The curves are derived from a theoretical 3B2S model with the parameters shown in the Table.

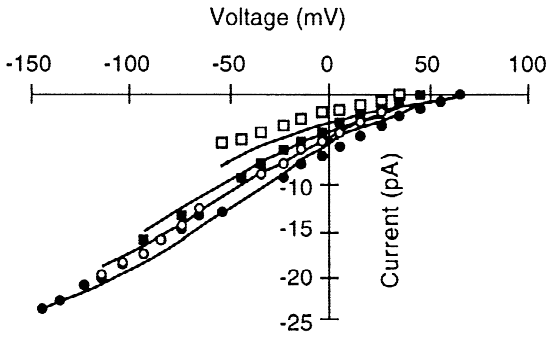

Fig. 6. The effect of increasing extracellular (*cis*) $CaCl_2$ concentration on the unitary-current *vs.* voltage relationships for the *rca* channel. The cytoplasmic side of the channel (*trans*) was exposed to 50 μM $CaCl_2$ while the extracellular side was exposed to 150 mM NaCl containing 0 (●), 1.5 (○), 3.5 (■) and 10.3 (□) mM free Ca^{2+} (as estimated by Geochem-PC), corresponding to a concentration range of 0 to 20 mM $CaCl_2$. Data are means from at least two bilayers. The curves are derived from a theoretical 3B2S model with the parameters shown in the Table.

tary conductance at positive voltages, decreased the unitary conductance at negative voltages and shifted the E_{rev} to more negative values (Fig. 4). The 3B2S model provided an adequate fit to the *I/V* curves obtained under these conditions. It fitted the currents observed at positive voltages well. It also simulated the decrease in unitary current observed at negative voltages as K^+ concentration was increased, but underestimated currents at extreme negative voltages at K^+ concentrations of 100 mM and below (Fig. 4*A*). The 3B2S model accurately fitted the relationship between E_{rev} and cytoplasmic K^+ concentration (Fig. 4*B*). The apparent P_{Ca}:P_K ratios calculated from the observed E_{rev} values using the assumptions of the GHK equation remained constant with changing cytoplasmic K^+ concentration (P_{Ca}:$P_K \approx 35$; Piñeros & Tester, 1997*a*).

The permeation of Ca^{2+} and K^+ through the pore of the *rca* channel was also investigated under ionic conditions approximating those encountered physiologically (Marschner, 1995), with 1 mM KCl plus 500 μM $CaCl_2$ at pH 5.5 on the extracellular (*cis*) side and 140 mM KCl plus 500 nM Ca^{2+} activity at pH 7.0 on the cytoplasmic (*trans*) side (Fig. 5). Under these conditions the 3B2S model fitted the observed *I/V* relationship adequately. It described the currents well at negative voltages, but the predicted E_{rev} (−47 mV) was more negative than the observed E_{rev} (−30 mV) and there was a minor discrepancy between the fitted and observed currents at positive voltages. The P_{Ca}:P_K calculated using the GHK equation was 23 under these conditions (Piñeros & Tester, 1997*a*).

When currents through the *rca* channel were assayed in biionic (*cis*:*trans*) 1 mM KCl:$CaCl_2$ the 3B2S model did not fit the observed *I/V* relationship (Fig. 7*A*). An adequate fit was only obtained if the free-energy values for U1 were increased and those for U2 were decreased for both K^+ and Ca^{2+}. This implies that the interactions between cations and the channel pore were different in this experimental series and suggests that there may be differences between individual *rca* channel proteins with superficially similar Ca^{2+} conductance, voltage-dependence and sensitivity to verapamil. This might occur through covalent modification of the *rca* channel protein or its interactions with other constituents of the membrane preparation.

Interactions Between Calcium and Sodium During Permeation

Sodium also permeates the *rca* channel (Piñeros & Tester, 1995). The free-energy profile for Na^+ permeation, and the interactions between Na^+ and Ca^{2+} within the pore of the *rca* channel were assessed from the effects of increasing Ca^{2+} activity in the presence of a fixed 150 mM Na^+ concentration at the extracellular (*cis*) face, while cytoplasmic (*trans*) Ca^{2+} activity was maintained at 50 μM (Fig. 6).

When the channel was assayed in biionic 50 μM $CaCl_2$ (*trans*):150 mM NaCl (*cis*), the channel exhibited a large inward (Na^+) conductance of about 100 pS and an E_{rev} of 58 ± 5 mV (Fig. 6). The E_{rev} value corresponds to an apparent P_{Ca}:P_{Na} of 67 calculated using the GHK equation according to Lewis (1979). Increasing the extracellular (*cis*) Ca^{2+} activity progressively reduced the amplitude of the inward current and its unitary conductance decreased from 105 to 30 pS.

In the absence of Ca^{2+} in the *trans* chamber, the

3B2S model for the *rca* channel fitted the *I/V* curve observed at voltages more negative than −50 mV, but underestimated the observed current at voltages between −30 and 40 mV. Under these conditions, the model suggested a slightly more positive value for E_{rev} (70 mV) than that determined by experimentation (58 mV). As the Ca^{2+} activity in the extracellular (*cis*) compartment was increased to 0.5, 1.5 and 3.5 mM, the 3B2S model fitted the *I/V* curves adequately, although it slightly underestimated the observed current at extreme negative voltages. When the *cis* Ca^{2+} activity was increased to 10.3 mM, the 3B2S model consistently overestimated the current. The 3B2S model predicted an increase in E_{rev} from 70 to 77 mV as the *cis* Ca^{2+} concentration was increased from zero to 10.3 mM, and an increase in the apparent P_{Ca}:P_{Na} from 40 to 50 (calculated according to GHK theory using the equations of Lewis, 1979).

Cation Selectivity of the *rca* Channel

In addition to Ca^{2+}, K^+ and Na^+, the *rca* channel is permeable to many other cations (Piñeros & Tester, 1995; White, 1998). These include cations that are relatively impermeant (Mg^{2+}, Mn^{2+}) or block (Cd^{2+}, Co^{2+}, Ni^{2+}) the L-type Ca^{2+} channels in animal cell membranes.

The permeation of a further nine divalent and three monovalent cations through the *rca* channel was investigated in experiments performed in biionic 1 mM (*cis*:*trans*) cation chloride:$CaCl_2$ (Figs. 7 and 8). A comparison of the apparent permeability ratios (calculated from E_{rev} values according to GHK theory using the equation of Fatt & Ginsborg, 1958) and the unitary conductance of the inward current (calculated between E_{rev} and −100 mV) relative to that observed in symmetrical 1 mM Ca^{2+} (Fig. 8) showed that divalent cations had a clear positive relationship between permeability and conductivity ratios, which was opposite to that shown by monovalent cations. This again indicates that the GHK equations are inappropriate to describe cation permeation through the *rca* channel. The selectivity sequence for divalent cations followed that of Sequence I in Sherry (1969), suggesting that permeating cations interacted with a weak field-strength site within the pore. Two contrasting selectivity sequences were obtained for monovalent cations, which reflects the strong interactions occurring between cations within the pore.

Predicted I/V Curves under Patch-Clamp Conditions

The 3B2S model described here can be used to predict net currents and cation fluxes through the *rca* channel at a given voltage under specified ionic conditions. It is instructive to compare the results obtained in the reduced PLB system to those observed in patch-clamp studies on

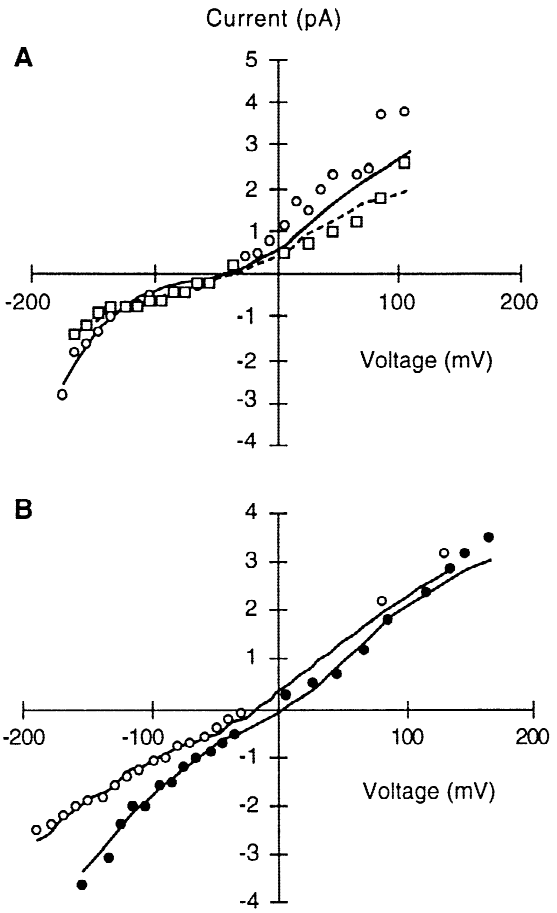

Fig. 7. Unitary-current *vs.* voltage relationships for the *rca* channel obtained with 1 mM $CaCl_2$ on the *trans* (cytoplasmic) side and (*A*) 1 mM KCl (□; $n = 5$ bilayers), 1 mM NaCl (○; $n = 6$ bilayers), (*B*) 1 mM $CaCl_2$ (●; $n = 29$ bilayers) or 1 mM $MgCl_2$ (○; $n = 3$ bilayers) on the *cis* (extracellular) side of the channel. The Ca^{2+} activity contaminating cation chloride solutions was assumed to be negligible. The solid curves are derived from a theoretical 3B2S model with the parameters for Ca^{2+} and Na^+ shown in the Table and parameters for Mg^{2+} of 0.7 (G1), 6.36 (G2), 3.91 (G3), 12.63 (U1) and 4.08 (U2) RT. The broken curve was derived using parameters of 0.09 (U1) and −2.28 (U2) for K^+ and −3.47 (U1) and −2.62 (U2) for Ca^{2+}.

protoplasts from plant cells. Two studies have characterized depolarization activated Ca^{2+}-currents across the plasma membrane of root-cell protoplasts (Thion et al., 1998; Kiegle et al., 1998). The 3B2S model was used to predict the unitary *I/V* relationship for the *rca* channel under the conditions employed in these patch-clamp experiments. However, since patch-clamp experiments frequently deploy Mg^{2+} on the cytoplasmic side of the plasma membrane and the *rca* channel is permeable to Mg^{2+}, it was necessary initially to determine the free-energy profile for Mg^{2+} permeation of the *rca* channel.

The free-energy profile for Mg^{2+} (legend to Fig. 7) was determined from the *I/V* relationship observed in biionic 1 mM (*cis*:*trans*) $MgCl_2$:$CaCl_2$ (Fig. 7*B*) assum-

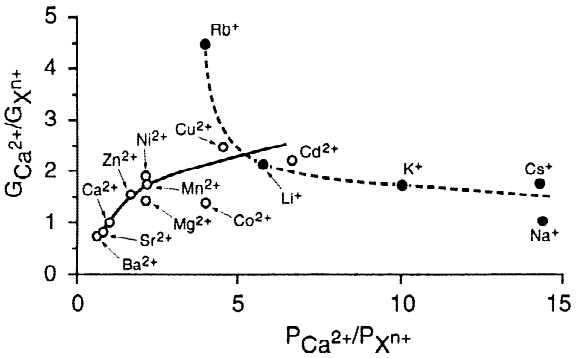

Fig. 8. Relationship between unitary conductance (calculated between E_{rev} and −100 mV and expressed relative to that observed in symmetrical 1 mM $CaCl_2$; G_{Ca}/G_x) and permeability ratios (P_{Ca}/P_x; estimated from E_{rev} using the GHK equation) for cations assayed in biionic 1 mM (*cis:trans*) cation chloride:$CaCl_2$. The mean unitary conductance in symmetrical $CaCl_2$ was 23.8 ± 0.8 pS (n = 29 bilayers) in experiments pertaining to divalent cations (solid line) and 33.7 ± 0.6 pS (n = 10 bilayers) in experiments pertaining to monovalent cations (broken line).

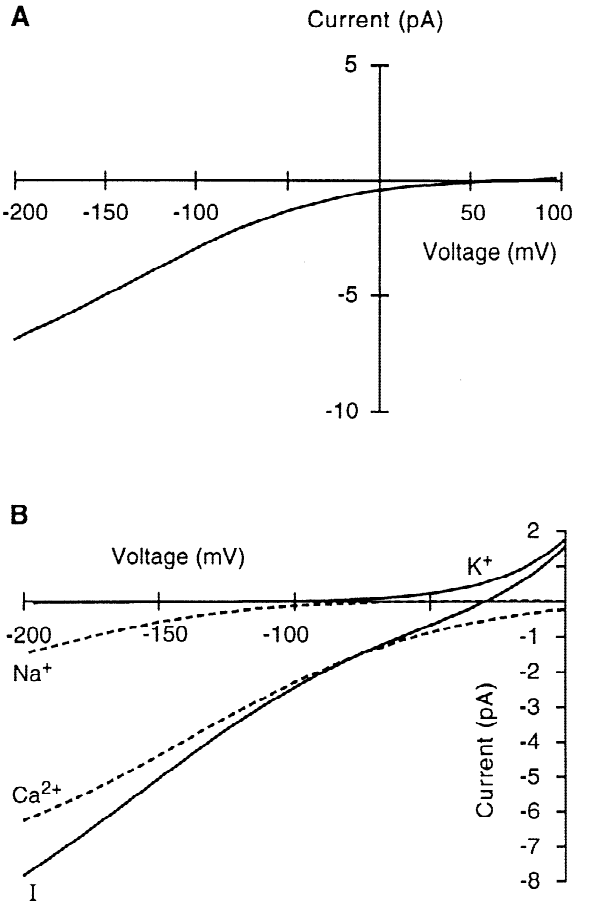

Fig. 9. (*A*) The predicted unitary-current *vs.* voltage (*I/V*) relationship for the *rca* channel when assayed under the patch-clamp ionic conditions documented by Thuleau et al. (1994). The estimated Ca^{2+} activity in the extracellular medium was 15.5 mM and the estimated Mg^{2+} activity in the pipette solution was 1.4 mM. (*B*) The predicted voltage-dependence of the unitary current (—) and net K^+ (—), Na^+ (- - - - -) and Ca^{2+} (- - - - -) currents when assayed under ionic conditions approximating those present physiologically (Marschner, 1995). The extracellular solution contained ionic activities of 0.904 mM K^+, 0.930 mM Na^+ and 0.696 mM Ca^{2+} and the cytoplasmic solution contained activities of 71.5 mM K^+, 3.5 mM Na^+ and 100 nM Ca^{2+}. The curves are derived from a theoretical 3B2S model with the parameters for K^+, Na^+ and Ca^{2+} shown in the Table and parameters for Mg^{2+} documented in the legend to Fig. 7.

ing the structural parameters and Ca^{2+} free-energy profile reported in the Table. Differences in permeation between Mg^{2+} and Ca^{2+} were attributed to a lower affinity for Mg^{2+} of the binding site (U2) closest to the extracellular side of the channel and higher free-energy barriers for the permeation of Mg^{2+} at both the center (G2) and extracellular side (G3) of the pore.

Under the ionic conditions typically used to study Ca^{2+} channels in plasma membrane of plant cells by patch-clamp techniques, the *rca* channel displayed nonlinear *I/V* relationships (Fig. 9*A*). The current reversal potential (E_{rev}) did not equal E_{Ca} since Mg^{2+} permeates the *rca* channel, but approximated the E_{rev} observed for currents through depolarization-activated Ca^{2+} channels in the plasma membrane of protoplasts assayed under comparable conditions (Thuleau et al., 1994; Kiegle et al., 1998). The predicted unitary conductance of the channel (determined between −100 and −50 mV) approximated 34 pS. This is greater than the unitary conductance determined for the depolarization-activated Ca^{2+} channel in the plasma membrane of cultured carrot cells, which was 13 pS in 40 mM $CaCl_2$ (Thuleau et al., 1994). However, the labile Ca^{2+}-selective channel formed when a phenylalkylamine-binding protein purified from cultured carrot cells is reconstituted into liposomes has a unitary conductance of 38 pS in (pipette: bath) 9:90 mM $CaCl_2$ (Thuleau et al., 1993).

Discussion

The Choice Of A 3B2S Model

Several models are available to describe ion permeation through channels (Nonner & Eisenberg, 1998; Levitt, 1999; McCleskey, 1999; Miller, 1999; White et al., 1999). These are based on the application of either (i) the GHK current equation, (ii) the concept of single-file movement through a rigid free-energy profile that can contain either one (single ion pore) or several (multi-ion pore) ions simultaneously, (iii) reaction-kinetic equations based on competitive translocation (dynamic-pore models), or (iv) solutions to the Poisson-Nernst-Planck (PNP) equations. Cation permeation through the *rca* channel cannot be described by the simple GHK current equation (*see* Introduction). The *I/V* relationships for the *rca* channel are not consistent with either an energy-barrier

model with a single binding site, since the channel displays anomalous mole fraction effects (Piñeros, 1995), or a dynamic-pore model, which predicts current saturation at extreme voltages. However, cation movement through the pore of the *rca* channel does behave as if it occurs in single file, with cations interacting with at least two binding sites within the pore and, in a multiply occupied pore, with each other. Thus, a minimal free-energy profile containing three energy barriers and two ion-binding sites was chosen to describe cation permeation through the *rca* channel. Indeed, similar 3B2S models have been used to describe cation permeation through other Ca^{2+} channels in the plasma membrane of both animal (e.g., Almers & McCleskey, 1984; Hess & Tsien, 1984; Hille, 1992; Yellen, 1993; Aidley & Stanfield, 1996; McCleskey, 1999) and plant cells (White & Ridout, 1999). The application of the PNP equations, or models based on molecular dynamic simulations (reviewed by Levitt, 1999), could not be attempted since there is no sequence or structural information available for the *rca* channel.

Adequacy of the Proposed 3B2S Model

In general the proposed 3B2S model fitted the observed *I/V* relationships adequately (but not perfectly) and described many of the notable permeation phenomena associated with the *rca* channel. In addition to resolving the apparent paradox arising from the variable cation permeabilities estimated using the GHK equation, the 3B2S model also accounted for the apparent plateau in unitary conductance at submillimolar $CaCl_2$ concentrations (Piñeros & Tester, 1997*a*; Fig. 1*F*) and the complex effects on *I/V* relationships observed when (i) extracellular Ca^{2+} activity was varied while maintaining a high cytoplasmic (*trans*) K^+ concentration (Fig. 3), (ii) when cytoplasmic K^+ was varied while maintaining a constant extracellular Ca^{2+} activity (Fig. 4), and (iii) when the extracellular Ca^{2+} concentration was increased in the presence of 150 mM NaCl while maintaining a constant cytoplasmic Ca^{2+} concentration (Fig. 6).

It was suggested earlier in this paper that the anomalous data might be explained, in part, by differences between individual channel proteins. This could account for the contrasting *I/V* relationships at extreme negative voltages in the experiments at low Ca^{2+} concentrations described in Fig. 1 and Fig. 2. It could also explain the need to alter the free-energy values for U1 and U2 for both K^+ and Ca^{2+} to fit the currents through the *rca* channel in the experimental series undertaken in biionic (*cis*:*trans*) 1 mM KCl:$CaCl_2$ (Fig. 7*A*). Such differences might arise through covalent modification of the *rca* channel protein or serendipitous interactions between the channel and other proteins or lipids present in the membrane preparation (Bell, 1986; Hille, 1992; Aidley & Stanfield, 1996).

Inferences for the Structure of the Channel Pore

Having demonstrated that, for the most part, the 3B2S model yields an adequate description of cation permeation through the *rca* channel, several inferences can be made regarding the structure of its pore. The model suggests considerable negative surface charge in the vestibules to the channel pore, which appears to be a general characteristic of cation channels (Hille, 1992; Aidley & Stanfield, 1996; Doyle et al., 1998). This serves to concentrate cations and, thereby, increases cation fluxes at low concentrations. This is illustrated by the high unitary conductances recorded in the presence of low $CaCl_2$ concentrations (Fig. 1*F*).

The model suggests that the outermost free-energy barriers and the cation binding sites are located at the extremes of the pore. The energy barriers for monovalent-cation permeation are not great and, in the absence of Ca^{2+}, the flux of monovalent cations through the *rca* channel is high (Piñeros & Tester, 1995). However, when Ca^{2+} is present at even micromolar concentrations, fluxes of monovalent cations through the *rca* channel are dramatically reduced (Figs. 3 and 6), reflecting the high affinity of the intrapore binding-sites for Ca^{2+} and the slow permeation of Ca^{2+} through the pore. The 3B2S model also suggests that the pore can be occupied by two cations simultaneously, and that cations within the pore will repel each other strongly. It has been suggested that channels exploit such electrostatic repulsion to promote cation conduction (Doyle et al., 1998).

The pore structure and the permeation and selectivity mechanisms proposed for the *rca* channel are similar to those proposed for several other Ca^{2+} channels in the membranes of both animal (Almers & McCleskey, 1984; Hess & Tsien, 1984; Friel & Tsien, 1989; Hille, 1992; Yellen, 1993; Aidley & Stanfield, 1996; McCleskey, 1999) and plant cells (White & Ridout, 1999). In these channels, the high affinity of intrapore binding sites for divalent cations, together with the strong repulsion between cations within the pore, provide the basis for the selective permeability of divalent cations.

Since the pharmacology of the *rca* channel (its sensitivity to trivalent cations, diltiazem and verapamil, but not its insensitivity to dihydropyridines) resembles L-type Ca^{2+} channels in animal cell membranes (Ranjeva et al., 1996; Piñeros & Tester, 1997*a*), it is perhaps instructive to compare the permeation models derived for the *rca* channel and L-type Ca^{2+} channels.

The magnitude of the unitary conductances observed for Ca^{2+} and Ba^{2+} are similar for the *rca* channel and L-type Ca^{2+} channels in animal cell membranes (Piñeros & Tester, 1997*a*). However, Mg^{2+} permeates the *rca* channel (Figs. 7 and 8) but frequently does not permeate L-type Ca^{2+} channels (Ranjeva et al., 1996) and the unitary conductances of the *rca* channel for monovalent cations are higher than those for L-type Ca^{2+} channels

when assayed at pH 6.0 (Nonner & Eisenberg, 1998). Thus, the structure of the pore of the *rca* channel must differ from that of the L-type channels. This has implications for strategies to identify the gene for the *rca* channel based on homologies with the selectivity filter of L-type Ca^{2+} channels. It is unlikely that the *rca* channel has the conserved quartet of glutamate residues (termed the EEEE locus; Aidley & Stanfield, 1996) that form the selectivity filter of animal Ca^{2+} channels and it is probably significant that this motif does not occur in the entire genome of the yeast *Saccharomyces cerevisiae.*

Differences in pore structure are also borne out by comparison of the respective free energy profiles for cation permeation. The affinities for Ca^{2+} of the cation binding sites within the pore of an unoccupied *rca* channel (K_ds of 6.6 and 2.8 μM for U1 and U2, respectively) are lower than those in an L-type Ca^{2+} channel from animal cells (K_d = 500 nM; Almers & McCleskey, 1984; Hess & Tsien, 1984; Friel & Tsien, 1989). But the affinity of the cation binding sites of an unoccupied *rca* channel for monovalent cations (K_ds between 1.3 and 5.7 mM) are higher than those in an L-type Ca^{2+} channel (K_d = 140 mM; Almers & McCleskey, 1984; Hess & Tsien, 1984). These properties account for the observation that, over the range of physiologically realistic ionic concentrations, the *rca* channel had a lower P_{Ca}:P_K ratio (17 to 41, when estimated following the assumptions of GHK theory; Piñeros & Tester, 1997*a*) than that of L-type Ca^{2+} channels (>3000; for a review *see* Hille, 1992). Furthermore they explain why the range of membrane potentials at which the current through the *rca* channel reverses is more negative than that reported for L-type Ca^{2+} channels (+50 to +80 mV; Hille, 1992). This property of the *rca* channel is likely to reflect the extremely negative resting potential and the magnitude of action potential depolarizations observed in plant cells. Thus, the pore structure of the *rca* channel may be particularly suited to the plant plasma membrane, allowing the *rca* channel to catalyze Ca^{2+} influx against a steep monovalent cation gradient at physiological membrane potentials (Fig. 9*B*).

Further Applications for the Permeation Model

Many biotic and abiotic stimuli result in substantial plasma membrane depolarizations that would activate the *rca* channel (Piñeros & Tester, 1997*a*). Such stimuli also elicit Ca^{2+} influx into root cells (Bush, 1995). The 3B2S model can be used to predict the net ionic fluxes through the *rca* channel at negative voltages under physiological ionic conditions (Fig. 9*B*). The majority of the inward current is predicted to be carried by Ca^{2+}, which justifies the classification of the *rca* channel as a Ca^{2+} channel. Little inward K^+ current is predicted, but there is a marked outward K^+ current at membrane potentials more positive than E_K.

In future simulations, the ability to predict ionic fluxes through the *rca* channel under physiological conditions, and to couple this with a kinetic model describing channel opening, will allow the role of the *rca* channel in depolarization-mediated Ca^{2+}-signaling to be examined theoretically (*cf.* White & Ridout, 1999). Modeling the gating kinetics of the *rca* channel is now a priority.

This work was supported by the Biotechnology and Biological Sciences Research Council, UK (PJW, MSR and MT), the Australian Research Council (MT), and the Overseas Postgraduate Research and University of Adelaide Scholarships awarded to MP. We thank Dr. Richard Napier and Dr. Soheila A.-H.-Mackerness (HRI) for their suggestions on the manuscript.

References

Aidley, D.J., Stanfield, P.R. 1996. Ion Channels. Molecules in Action. Cambridge University Press, Cambridge

Allen, G.J., Sanders, D., Gradmann, D. 1998. Calcium-potassium selectivity: kinetic analysis of current-voltage relationships of the open, slowly activating channel in the vacuolar membrane of *Vicia faba* guard-cells. *Planta* **204:**528–541

Almers, W., McCleskey, E.W. 1984. Nonselective conductance in calcium channels of frog muscle: Calcium selectivity in a single-file pore. *J. Physiol.* **353:**585–608

Alvarez, O., Villarroel, A., Eisenman, G. 1992. Calculation of ion currents from energy profiles and energy profiles from ion currents in multibarrier, multisite, multioccupancy channel models. *Methods Enzymol.* **207:**816–854

Bell, J. 1986. The sarcoplasmic potassium channel: Lipid effects. *In:* Ion Channel Reconstitution. C. Miller, editor. pp. 469–482. Plenum Press, New York

Bush, D.S. 1995. Calcium regulation in plant cells and its role in signaling. *Annu. Rev. Plant Physiol. Plant Molec. Biol.* **46:**95–122

Doyle, D.A., Cabral, J.M., Pfuetzner, R.A., Kuo, A., Gulbis, J.M., Cohen, S.L., Chait, B.T., MacKinnon, R. 1998. The structure of the potassium channel: Molecular basis of K^+ conduction and selectivity. *Science* **280:**69–77

Fatt, P., Ginsborg, B.L. 1958. The ionic requirements for the production of action potentials in crustacean muscle fibres. *J. Physiol.* **142:**516–543

Friel, D.D., Tsien, R.W. 1989. Voltage-gated calcium channels: Direct observation of the anomalous mole fraction effect at the single-channel level. *Proc. Natl. Acad. Sci. USA* **86:**5207–5211

Hess, P., Tsien, R.W. 1984. Mechanism of ion permeation through calcium channels. *Nature* **309:**453–456

Hille, B. 1992. Ionic Channels of Excitable Membranes. Sinauer Associates, Massachusetts

Kiegle, E., Haseloff, J., Tester, M. 1998. Calcium currents in GFP-expressing endodermal protoplasts from *Arabidopsis. In:* Abstracts of the 11th International Workshop in Plant Membrane Biology, Cambridge, p. 198

Levitt, D.G. 1999. Modeling of ion channels. *J. Gen. Physiol.* **113:**789–794

Lewis, C.A. 1979. Ion-concentration dependence of the reversal potential and the single channel conductance of ion channels at the frog neuromuscular junction. *J. Physiol.* **286:**417–445

Marschner, H. 1995. Mineral Nutrition of Higher Plants. Academic Press, London

McCleskey, E.W. 1999. Calcium channel permeation: A field in flux. *J. Gen. Physiol.* **113:**765–772

Miller, C. 1999. Ionic hopping defended. *J. Gen. Physiol.* **113:**783–787

Nonner, W., Eisenberg, B. 1998. Ion permeation and glutamate residues linked by Poisson-Nernst-Plank theory in L-type calcium channels. *Biophys. J.* **75:**1287–1305

Parker, D.R., Norvell, W.A., Chaney, R.L. 1995. GEOCHEM-PC: a chemical speciation program for IBM and compatible computers. *In:* Chemical Equilibrium and Reaction Models. R.H. Loeppert, A.P. Schwab and S. Goldberg, editors. pp. 253–269. Soil Science Society of America, Madison

Piñeros, M. 1995. Single channel characterization of a calcium selective channel from wheat roots. PhD thesis, University of Adelaide, Australia

Piñeros, M., Tester, M. 1995. Characterization of a voltage-dependent Ca^{2+}-selective channel from wheat roots. *Planta* **195:**478–488

Piñeros, M., Tester, M. 1997*a*. Calcium channels in higher plant cells: selectivity, regulation and pharmacology. *J. Exp. Bot.* **48:**551–577

Piñeros, M., Tester, M. 1997*b*. Characterization of the high-affinity verapamil binding site in a plant plasma membrane Ca^{2+}-selective channel. *J. Membrane Biol.* **157:**139–145

Ranjeva, R., Thuleau, P., Thion, L., Graziana, A., Mazars, C., Rossignol, M. 1996. Calcium entry into higher plant cells: voltage-operated plasma membrane-bound Ca^{2+} channels. *C R Acad. Sci. Paris* **319:**1063–1070

Sherry, H.S. 1969. The ion-exchange properties of zeolites. *In:* Ion Exchange. J. Marinsky, editor. pp. 89–133. Marcel Dekker, New York

Thion, L., Mazars, C., Nacry, P., Bouchez, D., Moreau, M., Ranjeva, R., Thuleau, P. 1998. Plasma membrane depolarization-activated calcium channels, stimulated by microtubule-depolymerizing drugs in wild-type *Arabidopsis thaliana* protoplasts, display constitutively large activities and a longer half-life in *ton 2* mutant cells affected in the organization of cortical microtubules. *Plant J.* **13:**603–610

Thuleau, P., Graziana, A., Ranjeva, R., Schroeder, J.I. 1993. Solubilized proteins from carrot (*Dawcus carota* L.) membranes bind calcium channel blockers and form calcium-permeable ion channels. *Proc. Natl. Acad. Sci. USA* **90:**765–769

Thuleau, P., Ward, J.M., Ranjeva, R., Schroeder, J.I. 1994. Voltage-dependent calcium-permeable channels in the plasma membrane of a higher plant cell. *EMBO J.* **13:**2970–2975

White, P.J. 1994. Characterization of a voltage-dependent cation-channel from the plasma membrane of rye (*Secale cereale* L.) roots in planar lipid bilayers. *Planta* **193:**186–193

White, P.J. 1997. Cation channels in the plasma membrane of rye roots. *J. Exp. Bot.* **48:**499–514

White, P.J. 1998. Calcium channels in the plasma membrane of root cells. *Ann. Bot.* **81:**173–183

White, P.J., Biskup, B., Elzenga, J.T.M., Homann, U., Thiel, G., Wissing, F., Maathuis, F.J.M. 1999. Advanced patch-clamp techniques and single-channel analysis. *J. Exp. Bot.* **50:**1037–1054

White, P.J., Ridout, M. 1995. The K^+ channel in the plasma membrane of rye roots has a multiple ion residency pore. *J. Membrane Biol.* **143:**37–49

White, P.J., Ridout, M.S. 1999. An energy-barrier model describing the permeation of monovalent and divalent cations through the maxi cation-channel in the plasma membrane of rye (*Secale cereale* L.) roots. *J. Membrane Biol.* **168:**63–75

Yellen, G. 1993. Structure and selectivity. *Nature* **366:**109–110